Revelation of a functional dependence of the sum of two uniaxial strengths/hardness on elastic work/total work of indentation

Dejun Ma
*Department of Mechanical Engineering, The Academy of Armored Forces Engineering,
Beijing 100072, People's Republic of China*

Taihua Zhang
*State Key Laboratory of Nonlinear Mechanics (LNM), Institute of Mechanics,
Chinese Academy of Sciences, Beijing 100080, People's Republic of China*

Chung Wo Ong[a]
*Department of Applied Physics and Materials Research Center, The Hong Kong Polytechnic
University, Hung Hom, Kowloon, Hong Kong, People's Republic of China*

Dimensional and finite element analyses were used to analyze the relationship between the mechanical properties and instrumented indentation response of materials. Results revealed the existence of a functional dependence of (engineering yield strength $\sigma_{E,y}$ + engineering tensile strength $\sigma_{E,b}$)/Oliver & Pharr hardness on the ratio of reversible elastic work to total work obtained from an indentation test. The relationship links up the Oliver & Pharr hardness with the material strengths, although the Oliver & Pharr hardness may deviate from the true hardness when sinking in or piling up occurs. The functional relationship can further be used to estimate the sum $\sigma_{E,y} + \sigma_{E,b}$ according to the data of an instrumented indentation test. The $\sigma_{E,y} + \sigma_{E,b}$ value better reflects the strength of a material compared to the hardness value alone. The method was shown to be effective when applied to aluminum alloys. The relationship can further be used to estimate the fatigue limits, which are usually obtained from macroscopic fatigue tests in different modes.

I. INTRODUCTION

There has been a long-lasting attempt to correlate the results obtained from indentation test with the fundamental mechanical properties of a material. More than 50 years ago, Tabor[1] first reported that the hardness H of some metals obtained from indentation tests by using a conical indenter was ~3 times a "representative yield stress (Y_o)," where Y_o was the true yield stress at a 0.08 true yield strain. This finding linked up the hardness with the standard material properties obtained from a uniaxial tensile/compressive test. Along with the development of depth-sensing indentation technique in the past decades, Tabor's conjecture was reexamined over a larger variety of materials. Cheng and Cheng[2] further introduced dimensional and finite element analyses (FEA) for conical indentation, and pointed out that when the ratio of yield strength to Young's modulus increased from 0.0002 to 0.1, the ratio H/Y_o would drop from about 2.8 to 1.7. Dao et al. also reported a similar trend,[3] leading to the conclusion that there was no simple proportional relationship between hardness and yield stress.

Another line of thought is to correlate the whole set of load–displacement data, rather than hardness value alone, with a group of fundamental material elasto-plastic properties, such as Young's modulus E, yield strength, Poisson's ratio ν, and stain-hardening exponent n.[3–5] However, Cheng and Cheng,[6] Capehard and Cheng,[7] and Tho et al.[8] pointed out that uniquely determining a set of the material parameters from a single set of load–displacement curves was unlikely. Therefore, more recently, a new approach has been developed: using two conical indenters of different half included angles to produce independent load–displacement curves for deriving material properties like yield stress and hardening coefficient etc.[9–12] In fact, more work is still required to examine the effectiveness and possible error of the method.
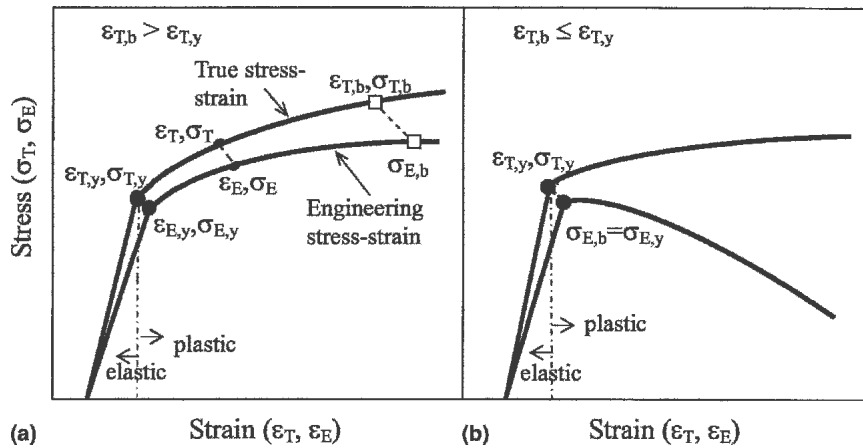
FIG. 1. Schematic diagrams showing the true and engineering stress–strain curves and the stress and strain quantities related to the study for the cases of (a) $\epsilon_{T,b} > \epsilon_{T,y}$ and (b) $\epsilon_{T,b} \leq \epsilon_{T,y}$.

In this paper, we report the results of a different approach. The method involves the symbols as shown in Fig. 1(a), where σ_T and ϵ_T are the true stress and strain, σ_E and ϵ_E the engineering stress and strain, and $\sigma_{T,y}$, $\epsilon_{T,y}$, $\sigma_{E,y}$, and $\epsilon_{E,y}$ the corresponding values at the yield point. The true stress and strain at the maximum engineering stress $\sigma_{E,b}$ (tensile strength) are $\sigma_{T,b}$ and $\epsilon_{T,b}$. Based on dimensional and finite element analyses, the proposed method leads to the establishment of a functional dependence of $(\sigma_{E,y} + \sigma_{E,b})$/Oliver & Pharr hardness on the reversible elastic work/total work ratio deduced from a set of load–unload curves. The method involves only the use of one conical indenter. The relationship links up the Oliver & Pharr hardness with the material strengths. It is also useful in estimating the sum $\sigma_{E,y} + \sigma_{E,b}$, where $\sigma_{E,y}$ and $\sigma_{E,b}$ are usually obtained from a standard uniaxial tensile test. This method is shown to be effective in estimating $\sigma_{E,y} + \sigma_{E,b}$ of aluminum alloys according to the published experimental results. The possibility of using the relationship in estimating the fatigue limits of materials is also proposed and discussed.

II. FUNCTIONAL DEPENDENCE OF $\sigma_{E,Y}$ AND $\sigma_{E,B}$ ON FUNDAMENTAL MATERIAL PARAMETERS

A. Functional dependence of $\sigma_{E,y}$ on fundamental material parameters

The uniaxial true stress–strain behavior of a solid to be analyzed is assumed to have a line with a slope of E in the elastic region, plus a curve obeying Hollomon's power law of hardening in the plastic region [Fig. 1(a)]. The function form is

$$\sigma_T = \begin{cases} E\,\epsilon_T, & \epsilon_T \leq \epsilon_{T,y} \\ \sigma_{T,y}(\epsilon_T/\epsilon_{T,y})^n, & \epsilon_T > \epsilon_{T,y} \end{cases} \quad , \quad (1)$$

where $\epsilon_{T,y} = \sigma_{T,y}/E$. In Appendix A, it is found that $\sigma_{E,y}$ can be expressed as a function of the fundamental material properties $\sigma_{T,y}$ (or $\epsilon_{T,y}$), E and ν.

$$\sigma_{E,y} = \sigma_{T,y}/\exp(2\nu\epsilon_{T,y}) = \sigma_{T,y}/\exp(2\nu\sigma_{T,y}/E) \quad . \quad (2)$$

B. Functional dependence of $\sigma_{E,b}$ on fundamental material properties

We derive the functional dependence of $\sigma_{E,b}$ on the fundamental material properties of the indented material for two cases. Case 1 is for the condition of $\epsilon_{T,b} \leq \epsilon_{T,y}$. Figure 1(b) provides a primary sketch for this case. When the engineering stress is increased to $\sigma_{E,y}$, the specimen reaches the yield point. For further increase in engineering strain, the corresponding engineering stress decreases subsequently. This means that the engineering yield stress $\sigma_{E,y}$ is the maximum in the engineering stress-strain curve, and hence is equal to $\sigma_{E,b}$, i.e., $\sigma_{E,b} = \sigma_{E,y} = \sigma_{T,y}/\exp(2\nu\epsilon_{T,y})$.

Case 2 is for the condition of $\epsilon_{T,b} > \epsilon_{T,y}$ as shown in Fig. 1(a). Appendix B shows that the true strain $\epsilon_{T,b}$ at maximum engineering stress $\sigma_{E,b}$ is

$$\epsilon_{T,b} = n[1 + (1 - 2\nu)\,\epsilon_{T,y}^{1-n}\,\epsilon_{T,b}^{n}] \quad . \quad (3)$$

Conceptually, $\epsilon_{T,b}$ can be regarded as a function of n, ν, and $\epsilon_{T,y}$, because when these three parameters are known, $\epsilon_{T,b}$ can normally be deduced by using Newton's method. Appendix B also shows that:

$$\sigma_{E,b} = \sigma_{T,b}/\exp[\epsilon_{T,b} + (2\nu - 1)\,\epsilon_{T,y}^{1-n}\,\epsilon_{T,b}^{n}]$$
$$= \sigma_{T,y}(\epsilon_{T,b}/\epsilon_{T,y})^{n}/\exp[\epsilon_{T,b} + (2\nu - 1)\,\epsilon_{T,y}^{1-n}\,\epsilon_{T,b}^{n}] \quad , \quad (4)$$

where $\sigma_{T,b} = \sigma_{T,y}(\epsilon_{T,b}/\epsilon_{T,y})^{n}$ is applied. Summarizing the results of the two cases:

$$\sigma_{E,b} =$$

$$\begin{cases} \sigma_{E,y} = \sigma_{T,y}/\exp(2\nu\epsilon_{T,y}) & , \epsilon_{T,b} \leqslant \epsilon_{T,y} \\ \dfrac{\sigma_{T,y}(\epsilon_{T,b}/\epsilon_{T,y})^n}{\exp[\epsilon_{T,b} + (2\nu - 1)\,\epsilon_{T,y}^{1-n}\,\epsilon_{T,b}^n]} & , \epsilon_{T,b} > \epsilon_{T,y} \end{cases},$$

(5)

indicating that in any case $\sigma_{E,b}$ is a function of fundamental material properties $\sigma_{T,y}$ (or $\epsilon_{T,y}$), E, ν, and n.

Combining Eqs. (2) and (5), one obtains an important corollary that the sum $\sigma_{E,y} + \sigma_{E,b}$ is a function of the fundamental material properties. This conclusion can be expressed with an implicit relationship like

$$\sigma_{E,y} + \sigma_{E,b} = f(\sigma_{T,y}, E, \nu, n) \quad , \tag{6}$$

or alternatively

$$\sigma_{T,y} = g[(\sigma_{E,y} + \sigma_{E,b}), E, \nu, n] \quad . \tag{7}$$

III. DIMENSIONAL AND FINITE ELEMENT ANALYSES OF HYPOTHETICAL INDENTATION TESTS

We use the Oliver & Pharr hardness in this study, which is defined as[11–13]:

$$H = P_m/A(h_{cm}) \quad , \tag{8}$$

where h_{cm} and $A(h_{cm})$ are the maximum contact depth and the related projected contact area measured at the peak load P_m. h_{cm} is defined according to the formula

$$h_{cm} = h_m - 0.75P_m/S_u \quad , \tag{9}$$

where h_m and S_u are the maximum displacement and unloading slope at P_m. The indenter is considered to be an elastic body. The contact interface between the indenter and the indented material is assumed to be frictionless. H is regarded to be the indentation response, and is a function of the elasto-plastic properties E, ν, $\sigma_{T,y}$, and n of the indented material; the elastic properties E_i and ν_i of the indenter; and the maximum indentation depth h_m. It can be expressed in an implicit form of

$$H = F_H(E, \nu, \sigma_{T,y}, n, E_i, \nu_i, h_m) \quad . \tag{10}$$

By substituting Eq. (7) into Eq. (10), H can be expressed as

$$H = F_H(E, \nu, g\,[(\sigma_{E,y} + \sigma_{E,b}), E, \nu, n], n, E_i, \nu_i, h_m)$$
$$= \Psi_H(E, \nu, (\sigma_{E,y} + \sigma_{E,b}), n, E_i, \nu_i, h_m) \quad . \tag{11}$$

Furthermore, according to Dao et al.'s analysis on sharp indentation,[3] the function can be simplified by introducing a reduced Young's modulus $E_r = 1/[(1 - \nu^2)/E + (1 - \nu_i^2)/E_i]$, which combines the overall elasticity effects

of the indenter and the indented material. Then, Eq. (11) becomes

$$H = \Phi_H[(\sigma_{E,y} + \sigma_{E,b}), n, E_r, h_m] \quad . \tag{12}$$

By applying the Π theorem of dimensional analysis, Eq. (12) can be transformed into the following dimensionless formula

$$H/E_r = \Gamma_H[(\sigma_{E,y} + \sigma_{E,b})/E_r, n] \quad . \tag{13}$$

Similar analysis can be conducted for the ratio of reversible elastic work to total work W_e/W. Analogous to Eq. (10), let us write $W_e/W = F_W(E, \nu, \sigma_{T,y}, n, E_i, \nu_i, h_m)$, where W_e and W are the areas under the unloading and loading curves respectively. An expression analogous to Eq. (13) is obtained, namely:

$$W_e/W = \Gamma_W[(\sigma_{E,y} + \sigma_{E,b})/E_r, n] \quad , \tag{14}$$

or

$$(\sigma_{E,y} + \sigma_{E,b})/E_r = \Gamma_S(W_e/W, n) \quad . \tag{15}$$

Substituting Eq. (15) into Eq. (13) to eliminate $\sigma_{E,y} + \sigma_{E,b}$, we obtain

$$H/E_r = \Gamma_H[\Gamma_S(W_e/W, n), n] = \Gamma_{HS}(W_e/W, n) \quad . \tag{16}$$

Further dividing Eq. (15) by Eq. (16), we obtain

$$(\sigma_{E,y} + \sigma_{E,b})/H = \Gamma_S(W_e/W, n)/\Gamma_{HS}(W_e/W, n)$$
$$= \Gamma_{SHW}(W_e/W, n) \quad . \tag{17}$$

In this study, we applied FEA to simulate the indentation tests to establish the explicit form of Eq. (17) for practical use. The commercial finite element code ABAQUS[14] was used for the computation processes because of its excellent capability for handling problems of strong nonlinearity and large displacement. The analysis was performed in the framework of continuum. The indenter was assumed to be a cone with a half-included angle of 70.3° and thus was geometrically equivalent to an ideal Berkovich indenter. The indented material was assumed to be isotropic and rate-independent. It obeyed the Von Mises yield criterion and pure isotropic hardening rule. The details of meshing are described elsewhere.[16,17] Four-node axisymmetric element type was used, with a size small enough to give more than 30 nodes around the point of contact. A sensitivity study was performed by reducing the element size by half. Results showed that the calculated peak load was not changed by more than 0.6%, confirming that the selected mesh size was fine enough for modeling the hypothetical conical indentation made on a semi-infinite solid.

Considering that $(\sigma_{E,y} + \sigma_{E,b})/H$ and W_e/W in Eq. (17) are independent on E_r and h_m, we may keep E_r and h_m unchanged by assigning fixed values to all the elastic properties (E, ν, E_i, ν_i) and the maximum indentation depth h_m. In fact, the indenter is assumed to be rigid, so

J. Mater. Res., Vol. 21, No. 4, Apr 2006

897

that E_i and ν_i can be removed for further simplicity. E, ν, and h_m were fixed at 70 GPa, 0.3, and 1 μm respectively, and hence E_r was calculated to be $E/(1 - \nu^2) = 70$ GPa$/(1 - 0.3^2) = 76.923$ GPa. Fifty-six combinations of $\sigma_{T,y}$ and n were selected, with their values in the ranges of 0.035–17.5 GPa and 0–0.45 respectively. For each combination, the corresponding value of $\sigma_{E,y} + \sigma_{E,b}$ was calculated from Eqs. (2) and (5) as shown in Table I. FEA was applied to simulate an indentation to produce the load-unload curves, from which the value of W_e/W was calculated, and the value of H was derived with the use of Eqs. (8) and (9). Finally, the value of $(\sigma_{E,y} + \sigma_{E,b})/H$ is determined and plotted against W_e/W in Fig. 2 with n as a parameter. More interpolated data were produced based on the matrix as shown in Table I, with the locations selected at 1/3 and 2/3 between every two adjacent n values and every two adjacent $\sigma_{T,y}$ values. This created 344 more combinations. Starting from a certain n (i.e., one of 0, 0.15, 0.3 and 0.45), the interpolated vales of $(\sigma_{E,y} + \sigma_{E,b})/H$ and W_e/W were obtained from the FEA results evaluated at four adjacent $\sigma_{T,y}$ values as listed in Table I, with the use of a third-order polynomial. Then, for a certain $\sigma_{T,y}$, more interpolated values of $(\sigma_{E,y} + \sigma_{E,b})/H$ and W_e/W were derived from the FEA results evaluated at $n = 0$, 0.15, 0.3 and 0.45, with the use of a third-order polynomial. All the FEA data and interpolated data are plotted in Fig. 2. It is found that $(\sigma_{E,y} + \sigma_{E,b})/H$ and W_e/W are correlated with a functional relationship, which is almost irrespective of the variation of n in a broad range. Hence, the value of $(\sigma_{E,y} + \sigma_{E,b})/H$ and W_e/W can be uniquely determined by the ratio of W_e/W.

In our previous work,[15] it was demonstrated that for $W_e/W < 0.25$, the Oliver & Pharr hardness may be very different from the real hardness ($\equiv$ indentation load/real projected contact area). In addition, the relationships
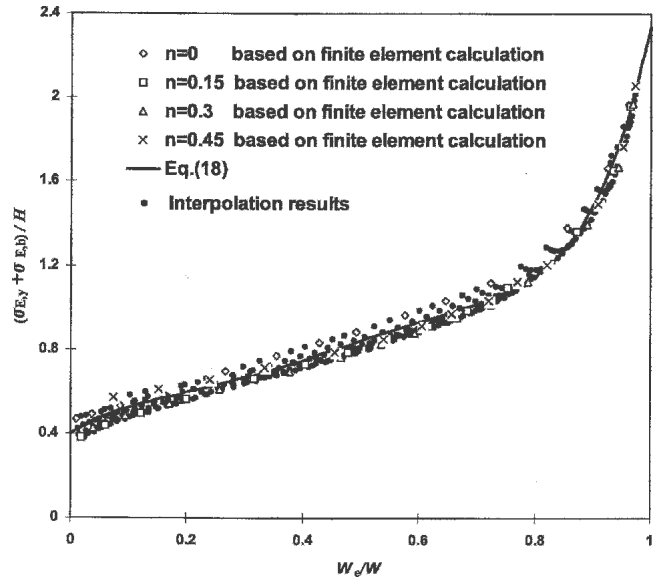

FIG. 2. Numerical values of $(\sigma_{E,y} + \sigma_{E,b})/H = \Gamma_{SHW}(W_e/W, n)$ against W_e/W for different values of n and the best fit to the data points expressed by Eq. (18).

established to correlate a true hardness with a representative yield are not applicable to the Oliver & Pharr hardness. Therefore, one needs to ask what the real meaning of the Oliver & Pharr hardness is, and how it is related to some fundamental properties like the intrinsic strengths of a material. The discovery of the above relationship gives possible answers by correlating the Oliver & Pharr hardness with the sum of two characteristic strengths of a material.

Figure 2 also shows the best fit to the data points produced with a polynomial of

$$(\sigma_{E,y} + \sigma_{E,b})/H = f(W_e/W) = a_0 + \sum_{i=1}^{6} a_i (W_e/W)^i \quad ,$$

(18)

where $a_0 = 0.40096$, $a_1 = 1.67585$, $a_2 = -5.64402$, $a_3 = 11.51201$, $a_4 = -0.15716$, $a_5 = -21.09499$, and $a_6 = 15.64194$. Equation (18) can also be rewritten in the form of:

$$\sigma_{E,y} + \sigma_{E,b} = H[f(W_e/W)] = H\left[a_0 + \sum_{i=1}^{6} a_i (W_e/W)^i\right] \quad .$$

(19)

It is noted that H in Eqs. (18) and (19) is not necessarily equal to the true hardness. For example, in the present study, we use Oliver & Pharr's definition, but it does not always give the true hardness, since piling up or sinking in could occur to make the value of h_{cm} deduced from Eq. (9) different from the true contact depth. The setting of the value of ϵ induces further uncertainty, e.g., for a conical indenter Oliver and Pharr use $\epsilon = 0.75$, but

TABLE I. Values of $\sigma_{T,y}$ n, and $(\sigma_{E,y} + \sigma_{E,b})$ used in numerical analysis (stresses in GPa).

$\sigma_{T,y}$	$\sigma_{E,y} + \sigma_{E,b}$			
	$n = 0$	$n = 0.15$	$n = 0.3$	$n = 0.45$
0.035	0.070	0.106	0.212	0.514
0.140	0.280	0.371	0.608	1.171
0.350	0.698	0.852	1.241	2.066
0.700	1.392	1.606	2.151	3.227
1.400	2.767	3.031	3.763	5.128
2.100	4.125	4.399	5.242	6.781
2.800	5.467	5.730	6.644	8.301
3.500	6.793	7.034	7.990	9.731
4.550	8.752	8.949	9.935	11.756
5.600	10.675	10.824	11.808	13.675
7.000	13.185	13.274	14.218	16.107
10.500	19.193	19.195	19.916	21.734
14.000	24.834	24.834	25.253	26.889
17.500	30.125	30.125	30.306	31.687

Sneddon uses $\epsilon = 0.72$. In fact, the meaning of Eq. (18) or Eq. (19) is to provide a relationship between the sum of the strengths $\sigma_{E,y} + \sigma_{E,b}$ and Oliver & Pharr's hardness through proper selection of the coefficients a_o to a_6, such that the value of $\sigma_{E,y} + \sigma_{E,b}$ can be deduced from the measured H value. It is further assumed that the indentation is deep enough such that the indenter is considered to possess the ideal Berkovich geometry with a projected area of $A(h_{cm}) = 24.5\ h_{cm}^2$. This is true in the present study since the experimental data are selected from indentation tests with maximum displacement $h_m > 8\ \mu m$, which normally exceeds the bluntness of an indenter tip.

Denoting $(\sigma_{E,y} + \sigma_{E,b})_e$ as the result calculated from Eqs. (2) and (5) based on the model of the material properties, and $(\sigma_{E,y} + \sigma_{E,b})_f$ as the result obtained from Eq. (19) based on the finite element simulations, the ratio $(\sigma_{E,y} + \sigma_{E,b})_f/(\sigma_{E,y} + \sigma_{E,b})_e$ would reflect the consistency between the two values. Referring to Eqs. (17) and (19), $(\sigma_{E,y} + \sigma_{E,b})_f/(\sigma_{E,y} + \sigma_{E,b})_e$ would depend on W_e/W and n, namely, in implicit form:

$$(\sigma_{E,y} + \sigma_{E,b})_f/(\sigma_{E,y} + \sigma_{E,b})_e =$$
$$\{H[f(W_e/W)]\}/\{H\ \Gamma_{SHW}(W_e/W, n)\} = \Gamma_{fe}(W_e/W, n) \quad . \tag{20}$$

The numerical results of $\Gamma_{fe}(W_e/W, n)$ are calculated and plotted in Fig. 3. A result of 1 refers to a perfect match, while most data points lie within a narrow band of $\pm 14\%$.
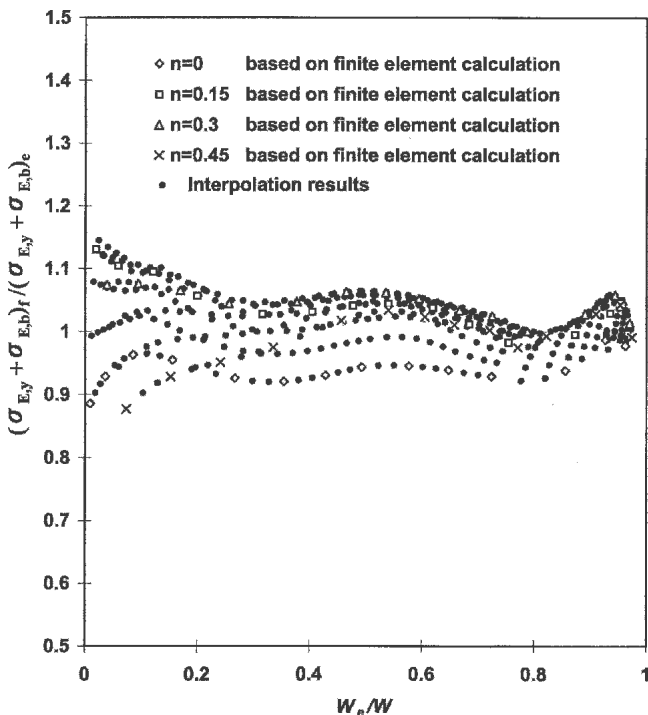

FIG. 3. Numerical values of $(\sigma_{E,y} + \sigma_{E,b})_f/(\sigma_{E,y} + \sigma_{E,b})_e = \Gamma_{fe}(W_e/W, n)$ against W_e/W for different values of n.

IV. EXPERIMENTAL EVALUATION OF THE THEORY

We referred to some published data of stress–strain tests and indentation tests for two aluminum alloys 6061-T6511 and 7075-T651[3] to examine the effectiveness of the theory. The parameters extracted from the stress–strain curves of uniaxial tests, and the sum of two strengths $(\sigma_{E,y} + \sigma_{E,b})_t$ obtained from uniaxial test with the use of Eqs. (2) and (5) are listed in Table II.

On the other hand, the results of the indentation tests are summarized in Table III. h_m is evaluated from the equation $h_m = (P_m/C)^{1/2}$, with C being the loading curvature. The hardness H is calculated from Eqs. (8) and (9). The sum of the two characteristic strengths is estimated from Eq. (19) and is denoted as $(\sigma_{E,y} + \sigma_{E,b})_i$ with the subscript i referring to a quantity deduced from an indentation test. The last column of Table III shows the relative error $Re = [(\sigma_{E,y} + \sigma_{E,b})_i - (\sigma_{E,y} + \sigma_{E,b})_t]/(\sigma_{E,y} + \sigma_{E,b})_i$. It is found that the values of R_e are located within a reasonably narrow range, supporting the effectiveness of the theory. Nevertheless, more experimental work should be done in the next stage to investigate a broader class of materials for further confirmation of the universal effectiveness of the method.

V. APPLICATIONS OF THE FUNCTIONAL DEPENDENCE OF $(\sigma_{E,y} + \sigma_{E,b})/H$ ON W_e/W

In this section, we propose two possible applications based on the functional dependence of $(\sigma_{E,y} + \sigma_{E,b})/H$ on W_e/W.

First, the relationship can be used to deduce the sum $\sigma_{E,y} + \sigma_{E,b}$ of a material from H and W_e/W measured in an indentation test. This quantity reflects the fundamental property of a material since it is composed of two characteristic material strengths. However, in general, it does not vary coherently with hardness, although the latter is widely referred to as a material performance indicator in practice. This remark is clearly illustrated through Fig. 4, which shows how the ratio $[(\sigma_{E,y} + \sigma_{E,b})_1/(\sigma_{E,y} + \sigma_{E,b})_2]/[H_1/H_2]$ varies with $(W_e/W)_1$ and $(W_e/W)_2$, with the subscripts "1" and "2" referring to the quantities of two materials respectively. According to Eq. (18), the ratio $[(\sigma_{E,y} + \sigma_{E,b})_1/(\sigma_{E,y} + \sigma_{E,b})_2]/[H_1/H_2]$ can be expressed as $f[(W_e/W)_1]/f[(W_e/W)_2]$, i.e., a function of $(W_e/W)_1$ and

TABLE II. Experimental results of uniaxial tests for two aluminum alloys.

Material	E (GPa)	υ	$\sigma_{T,y}$(MPa)	n	$(\sigma_{E,y} + \sigma_{E,b})_t$ (MPa)
Al 6061 − T6511	66.8	0.33	284	0.08	615.4
Al 7075 − T651	70.1	0.33	500	0.122	1125.6

CAMBRIDGE JOURNALS

http://journals.cambridge.org

J. Mater. Res., Vol. 21, No. 4, Apr 2006

Downloaded: 04 Oct 2013

IP address: 158.132.161.103

899

TABLE III. Experimental data of indentation tests for two aluminum alloys with a fixed P_m = 3N.

| Material	C (GPa)	h_m (μm)	S_u (N/mm)	H (GPa)	W_e/W	$f(W_e/W)$	$(\sigma_{E,y} + \sigma_{E,b})_i$ (MPa)	Re (%)
Al 6061 − T6511								
Test 1	27.4	10.46	4768	1.226	0.098	0.5216	639.8	3.8
Test 2	28.2	10.31	4800	1.263	0.095	0.5189	655.5	6.1
Test 3	27.2	10.50	4794	1.217	0.096	0.5198	632.4	2.7
Test 4	27.3	10.48	4671	1.224	0.111	0.5328	652.3	5.7
Test 5	27.0	10.54	4762	1.208	0.111	0.5328	643.6	4.4
Test 6	27.6	10.43	4491	1.243	0.109	0.5312	660.3	6.8
Al 7075 − T651								
Test 1	42.0	8.45	3665	1.993	0.167	0.5745	1145.2	1.7
Test 2	40.9	8.56	3658	1.938	0.162	0.5711	1106.6	−1.7
Test 3	42.3	8.42	3654	2.010	0.168	0.5752	1156.0	2.6
Test 4	43.1	8.34	3744	2.043	0.164	0.5725	1169.5	3.8
Test 5	43.5	8.30	3789	2.060	0.161	0.5704	1174.7	4.2
Test 6	44.6	8.20	3706	2.123	0.169	0.5759	1222.6	7.9
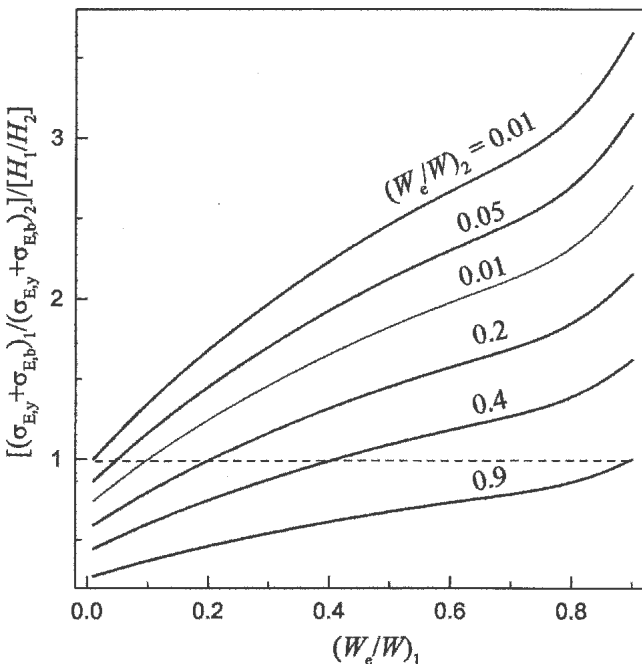
FIG. 4. Plot of the ratio $[(\sigma_{E,y} + \sigma_{E,b})_1/(\sigma_{E,y} + \sigma_{E,b})_2]/[H_1/H_2]$ as a function of $(W_e/W)_1$ and $(W_e/W)_2$, with the subscript "1" and "2" referring to the quantities of two materials.

$(W_e/W)_2$. It is found that $[(\sigma_{E,y} + \sigma_{E,b})_1/(\sigma_{E,y} + \sigma_{E,b})_2]/[H_1/H_2]$ could deviate significantly from 1. As a numerical example, when $(W_e/W)_1 = 0.6$ and $(W_e/W)_2 = 0.05$, the values of $f[(W_e/W)_1]$ and $f[(W_e/W)_2]$ are 0.93 and 0.47, respectively. This gives a ratio of $[(\sigma_{E,y} + \sigma_{E,b})_1/(\sigma_{E,y} + \sigma_{E,b})_2]/[H_1/H_2] = 1.97$, which is much greater than 1. This verifies that comparison of hardnesses of two materials alone is not sufficient to reflect the difference between their strengths.

Second, the $\sigma_{E,y} + \sigma_{E,b}$ value deduced from the method can further be used to estimate the fatigue limits of some structure steels. At present, there are many empirical relationships established for correlating the fatigue limits with $\sigma_{E,b}$, but obviously the fatigue behavior should also be related to the yield stress $\sigma_{E,y}$.[18] A more reasonable approach is to link up the fatigue limits with some quantity containing both of them. According to Ref. 19, the fatigue limits measured with symmetric cycling stress in tensile-compressive mode, rotating-bending mode, and shearing stress mode are estimated to be

$$\sigma_{-1l} = 0.23 \, (\sigma_{E,y} + \sigma_{E,b}) \quad , \quad (21)$$

$$\sigma_{-1} = 0.27 \, (\sigma_{E,y} + \sigma_{E,b}) \quad , \quad (22)$$

$$\tau_{-1} = 0.55 \, \sigma_{-1} = 0.1485 \, (\sigma_{E,y} + \sigma_{E,b}) \quad . \quad (23)$$

The corresponding quantities measured with pulsating cycling stress in the three modes are

$$\sigma_{ol} = 1.42\sigma_{-1l} = 0.3266 \, (\sigma_{E,y} + \sigma_{E,b}) \quad , \quad (24)$$

$$\sigma_o = 1.33\sigma_{-1} = 0.3591 \, (\sigma_{E,y} + \sigma_{E,b}) \quad , \quad (25)$$

$$\tau_o = 1.50\tau_{-1} = 0.22275 \, (\sigma_{E,y} + \sigma_{E,b}) \quad . \quad (26)$$

Some experimental results cited from Ref. 20 for middle or low strength steels are shown in Table IV to show the effectiveness of Eqs. (21)–(26). In Table IV, $(\sigma_{-1l})_{exp}$, $(\sigma_{-1})_{exp}$, $(\tau_{-1})_{exp}$, $(\sigma_{0l})_{exp}$, $(\sigma_0)_{exp}$, and $(\tau_0)_{exp}$ denote the experimental data; σ_{-1l}, σ_{-1}, τ_{-1}, σ_{0l}, σ_0, and τ_0 denote the estimated fatigue limits deduced from the respective Eqs. (21)–(26); and "%err" represents the relative errors of the estimated fatigue limit. For the purpose of evaluating the fatigue limits of materials, it is conceivable that Eqs. (21)–(26) can give reasonably good estimates. Because our present method provides an effective means to estimate the sum $\sigma_{E,y} + \sigma_{E,b}$, it would also be useful for estimating the fatigue limits for the cases when facilities for standard fatigue tests are not conveniently available. At last, we need to point out that the empirical Eqs. (21)–(26) are suggested for middle or low strength steels

TABLE IV. Experimental and evaluated fatigue limits for some steels (unit in MPa, stress cycling number $N = 10^7$).

Type of steel	$\sigma_{E,y}$	$\sigma_{E,b}$	$(\sigma_{-1I})_{exp}$	σ_{-1I}	%err σ_{-1I}	$(\sigma_{-1})_{exp}$	σ_{-1}	%err σ_{-1}	$(\tau_{-1})_{exp}$
Carbon steel									
St. 34	220	340	120	129	6.8	160	151	−5.8	90
St. 38	240	380	130	143	8.8	180	167	−7.5	100
St. 42	260	420	140	156	10.5	200	184	−8.9	120
St. 50	300	500	180	184	2.2	240	216	−11.5	140
St. 52-3	360	520	200	202	1.2	280	238	−17.8	160
St. 60	340	600	200	216	7.5	280	254	−10.3	160
St. 70	370	700	230	246	6.5	320	289	−10.8	190
Heat-treated steel									
C 25	310	500	210	186	−12.7	260	219	−18.9	150
C 35	370	600	230	223	−3.1	290	262	−10.7	170
C 45	400	650	250	242	−3.5	320	284	−12.9	180
C 60	490	750	290	285	−1.7	360	335	−7.5	210
40Mn4	550	800	310	311	0.2	390	365	−7.0	230
37MnSi5	650	900	350	357	1.8	440	419	−5.1	260
42MnV7	800	1000	380	414	8.2	480	486	1.2	290
40Cr4	650	900	360	357	−1.0	440	419	−5.1	260
50CrV4	900	1100	400	460	13.0	510	540	5.6	310
25CrMo4	550	800	310	311	0.2	380	365	−4.3	210
34CrMo4	650	900	360	357	−1.0	440	419	−5.1	250
42CrMo4	800	1000	380	414	8.2	480	486	1.2	290
50CrMo4	900	1100	430	460	6.5	510	540	5.6	310
30CrMoV9	1050	1250	450	529	14.9	560	621	9.8	340
36CrNiMo4	800	1000	390	414	5.8	480	486	1.2	280

Type of steel	τ_{-1}	%err τ_{-1}	$(\sigma_{0I})_{exp}$	σ_{0I}	%err σ_{0I}	$(\sigma_0)_{exp}$	σ_0	%err σ_0	$(\tau_0)_{exp}$	τ_0	%err τ_0
Carbon steel											
St. 34	83	−8.2	190	183	−3.9	240	201	−19.3	130	125	−4.2
St. 38	92	−8.6	210	202	−3.7	260	223	−16.8	150	138	−8.6
St. 42	101	−18.8	240	222	−8.1	300	244	−22.9	160	151	−5.6
ST. 50	119	−17.8	300	261	−14.8	370	287	−28.8	190	178	−6.6
St. 52-3	131	−22.4	330	287	−14.8	410	316	−29.7	220	196	−12.2
St. 60	140	−14.6	340	307	−10.7	430	338	−27.4	220	209	−5.1
St. 70	159	−19.6	370	349	−5.9	490	384	−27.5	260	238	−9.1
Heat-treated steel											
C 25	120	−24.7	310	265	−17.2	390	291	−34.1	200	180	−10.8
C 35	144	−18.0	370	317	−16.8	440	348	−26.3	250	216	−15.7
C 45	156	−15.4	400	343	−16.6	490	377	−30.0	270	234	−15.4
C 60	184	−14.0	480	405	−18.5	550	445	−23.5	310	276	−12.2
40Mn4	200	−14.7	510	441	−15.7	590	485	−21.7	280	301	6.9
37MnSi5	230	−13.0	580	506	−14.6	680	557	−22.2	410	345	−18.8
42MnV7	267	−8.5	640	588	−8.9	740	646	−14.5	460	401	−14.7
40Cr4	230	−13.0	600	506	−18.5	670	557	−20.4	400	345	−15.9
50CrV4	297	−4.4	680	653	−4.1	800	718	−11.4	480	446	−7.7
25CrMo4	200	−4.8	520	441	−17.9	590	485	−21.7	270	301	10.2
34CrMo4	230	−8.6	590	506	−16.5	680	557	−22.2	390	345	−13.0
42CrMo4	267	−8.5	640	588	−8.9	740	646	−14.5	450	401	−12.2
50CrMo4	297	−4.4	720	653	−10.2	790	718	−10.0	480	446	−7.7
30CrMoV9	342	0.5	760	751	−1.2	880	826	−6.5	480	512	6.3
36CrNiMo4	267	−4.8	650	588	−10.6	730	646	−12.9	450	401	−12.2

only. If it is applied to high strength steels, the fatigue limits may be overestimated.

VI. CONCLUSIONS

In this study, the existence of a functional dependence of $(\sigma_{E,y} + \sigma_{E,b})$/indentation hardness on reversible elastic work to total work ratio was established by using dimensional and finite element analyses. The published experimental data of uniaxial tests and indentation tests made on aluminum alloys 6061-T6511 and 7075-T651 support the effectiveness of the theory. The establishment of the relationship gives a physical explanation to the Oliver & Pharr hardness, which may be very different

J. Mater. Res., Vol. 21, No. 4, Apr 2006

901

from the real hardness in some situations. One important application of the functional relationship is for the determination the sum of the yield strength and tensile strength based on the results of an indentation test. The sum of the two strengths obtained was considered to be more suitable for reflecting the strength level of different materials since it is considered to be more physically meaningful than the indentation hardness. Another important application of the functional relationship is to estimate the fatigue limits of some structural steel by using the data of indentation test.

ACKNOWLEDGMENT

REFERENCES

1. D. Tabor: *The Hardness of Metals* (Oxford, London, UK, 2000), pp.104–106.
2. Y-T. Cheng and C-M. Cheng: Scaling approach to conical indentation in elastic-plastic solids with work hardening. *J. Appl. Phys.* **84,** 1284 (1998).
3. M. Dao, N. Chollacoop, K.J. Van Vliet, T.A. Venkatesh, and S. Suresh: Computational modeling of the forward and reverse problems in instrumented sharp indentation. *Acta Mater.* **49,** 3899 (2001).
4. A.E. Giannakopoulos and S. Suresh: Deterministic of elastoplastic properties by instrumented sharp indentation. *Scripta Mater.* **40,** 1191 (1999).
5. K. Zeng and C.H. Chiu: An analysis of load-penetration curves from instrumented indentation. *Acta Mater.* **49,** 3539 (2001).
6. Y-T. Cheng and C-M. Cheng: Can stress–strain relationships be obtained from indentation curves using conical and pyramidal indenters? *J. Mater. Res.* **14,** 3493 (1999).
7. T.W. Capehart and Y-T. Cheng: Determining constitutive models from conical indentation: Sensitivity analysis. *J. Mater. Res.* **18,** 827 (2003).
8. K.K. Tho, S. Swaddiwudhipong, Z.S. Liu, K. Zeng, and J. Hua: Uniqueness of reverse analysis from conical indentation tests. *J. Mater. Res.* **19,** 2498 (2004).
9. J.L. Bucaille, S. Stauss, E. Felder, and J. Michler: Determination of plastic properties of metals by instrumented indentation using different sharp indenters. *Acta Mater.* **51,** 1663 (2003).
10. Y. Cao, X. Qian, J. Lu, and Z. Yao: An energy-based method to extract plastic properties of metal materials from conical indentation tests. *J. Mater. Res.* **20,** 1194 (2005).
11. W.C. Oliver and G.M. Pharr: An improved technique for determining hardness and elastic modulus using load and displacement sensing indentation experiments. *J. Mater. Res.* **7,** 1564 (1992).
12. G.M. Pharr, W.C. Oliver, and F.R. Brotzen: On the generality of the relationship among contact stiffness, contact area, and elastic modulus during indentation. *J. Mater. Res.* **7,** 613 (1992).
13. W.C. Oliver and G.M. Pharr: Measurement of hardness and elastic modulus by instrumented indentation: Advances in understanding and refinements to methodology. *J. Mater. Res.* **19,** 3 (2004).
14. ABAQUS: Version 6.2 (Hibbitt, Karlsson & Sorensen, Inc., Pawtucket, RI, 2001).
15. D. Ma, T. Zhang, and C.W. Ong: Evaluation of effectiveness of representative methods for determining Young's modulus and hardness from instrumented indentation data. *J. Mater. Res.* **21,** 225 (2006).
16. D. Ma, C.W. Ong, and S.F. Wong: New relationship between Young's modulus and nonideally sharp indentation parameters. *J. Mater. Res.* **19,** 2144 (2004).
17. D. Ma, C.W. Ong, J. Lu, and J. He: Methodology for the evaluation of yield strength and hardening behavior of metallic materials by indentation with spherical tip. *J. Appl. Phys.* **94,** 288 (2003).
18. Y. Song: *Design, Selection and Prediction of Metallic Materials* (Mechanical Industry Press, Beijing, China, 1998), p. 443.
19. H. Xu: *Design of Fatigue Strength* (Mechanical Industry Press, Beijing, China, 1981), p. 45 (in Chinese).
20. M. Li, O. Buxbaum, and H. Lowak: *Structure Design Against Fatigue* (Mechanical Industry Press, Beijing, China, 1987), p. 31 (in Chinese).

APPENDIX A: FUNCTIONAL DEPENDENCE OF $\sigma_{E,y}$ ON FUNDAMENTAL MATERIAL PROPERTIES

In a tensile test, when the load is increased from zero to a certain value, the transverse cross-sectional radius and area vary from the unstressed values r_o and $A_o = \pi r_o^2$ to the instantaneous values r and $A = \pi r^2$. At this moment, the engineering stress is

$$\sigma_E = F/A_o = (F/A)(A/A_o) = \sigma_T(A/A_o) = \sigma_T(r/r_o)^2 \quad . \tag{A1}$$

The r/r_o is achieved from the definition of true radial strain

$$\epsilon_{T,r} = \int_{r_o}^{r} dr/r = \ln(r/r_o) \quad ,$$

which is also equal to $-\nu \epsilon_T$ in the elastic regime, such that

$$r/r_o = \exp(-\nu \epsilon_T) \quad \text{and} \quad , \tag{A2}$$

$$A/A_o = (r/r_o)^2 = \exp(-2\nu\epsilon_T) \quad . \tag{A3}$$

Substituting Eq. (A3) into Eq. (A1), one obtains:

$$\sigma_E = \sigma_T/\exp(2\nu\epsilon_T) \quad , \tag{A4}$$

and $\quad \sigma_{E,y} = \sigma_{T,y}/\exp(2\nu\epsilon_{T,y}) = \sigma_{T,y}/\exp(2\nu\sigma_{T,y}/E) \quad . \tag{A5}$

The latter is Eq. (2) in the text.

APPENDIX B: FUNCTIONAL DEPENDENCE OF $\epsilon_{T,b}$ AND $\sigma_{E,b}$ ON FUNDAMENTAL MATERIAL PROPERTIES

For an uniaxial stress-strain relation, the true strain ϵ_T in the plastic regime should consist of two parts, i.e.

elastic strain $\epsilon_T^e = \sigma_T/E$ and plastic strain $\epsilon_T^p = \epsilon_T - \epsilon_T^e = \epsilon_T - \sigma_T/E$. According to the theory of elasticity, the radial strain associated with the former is $\epsilon_{T,r}^e = -\nu\sigma_T/E$. From the constant-volume condition for plastic deformation, the radial strain associated with the plastic strain ϵ_T^p is $\epsilon_{T,r}^p = -0.5\epsilon_T^p = -0.5(\epsilon_T - \sigma_T/E)$. Summarizing these results, the overall true radial strain $\epsilon_{T,r}$ is expressed as:

$$\begin{aligned} \epsilon_{T,r} &= \epsilon_{T,r}^e + \epsilon_{T,r}^p \\ &= -[\nu\sigma_T/E + 0.5(\epsilon_T - \sigma_T/E)] \\ &= -[0.5\ \epsilon_T + (\nu - 0.5)\sigma_T/E] \quad . \end{aligned} \tag{A6}$$

After replacing σ_T with $\sigma_{T,y}(\epsilon_T/\epsilon_{T,y})^n$, Eq. (A6) becomes:

$$\epsilon_{T,r} = -[0.5\ \epsilon_T + (\nu - 0.5)\ \epsilon_{T,y}^{1-n}\ \epsilon_T^n] \quad . \tag{A7}$$

When the engineering stress reaches the maximum value, the increase in load for further elongating the specimen is compensated with the reduction in cross-sectional area, namely:

$$dF = d(\sigma_T A) = \sigma_T\ dA + A\ d\sigma_T = 0 \quad , \tag{A8}$$

$$-dA/A = d\sigma_T/\sigma_T \quad . \tag{A9}$$

The two sides of Eq. (A9) are $-dA/A = -2dr/r = -2\ d\epsilon_{T,r}$ and $d\sigma_T/\sigma_T = d[\sigma_{T,y}(\epsilon_T/\epsilon_{T,y})^n]/[\sigma_{T,y}\ (\epsilon_T/\epsilon_{T,y})^n] = n\ d\epsilon_T/\epsilon_T$, respectively, so that:

$$-2\ d\epsilon_{T,r} = n\ d\epsilon_T/\epsilon_T \quad . \tag{A10}$$

By substituting Eq. (A7) into Eq. (A10), at $\epsilon_T = \epsilon_{T,b}$, Eq. (A10) is transformed to become Eq. (3):

$$\epsilon_{T,b} = n[1 + (1 - 2\nu)\ \epsilon_{T,y}^{1-n}\ \epsilon_{T,b}^{1-n}] \quad . \tag{A11}$$

From Eq. (A7), when $\epsilon_{T,b} > \epsilon_{T,y}$, the radial strain $\epsilon_{T,r}$ and engineering stress $\sigma_{E,b}$ at $\epsilon_T = \epsilon_{T,b}$ can be determined as:

$$\begin{aligned} \epsilon_{T,r}\ |_{\epsilon_T = \epsilon_{T,b}} &= -[0.5\ \epsilon_T + (\nu - 0.5)\epsilon_{T,y}^{1-n}\epsilon_T^n]\ |_{\epsilon_T = \epsilon_{T,b}} \\ &= -[0.5\ \epsilon_{T,b} + (\nu - 0.5)\epsilon_{T,y}^{1-n}\epsilon_{T,b}^n] \quad , \end{aligned} \tag{A12}$$

and

$$\begin{aligned} \sigma_{E,b} &= \frac{F|_{\epsilon_T = \epsilon_{T,b}}}{A_o} = \frac{F|_{\epsilon_T = \epsilon_{T,b}}}{A|_{\epsilon_T = \epsilon_{T,b}}}\ \frac{A|_{\epsilon_T = \epsilon_{T,b}}}{A_o} \\ &= \sigma_T|_{\epsilon_T = \epsilon_{T,b}} \left(\frac{r}{r_o}\right)^2 |_{\epsilon_T = \epsilon_{T,b}} \\ &= \sigma_{T,b}\ \exp(2\epsilon_{T,r}|_{\epsilon_T = \epsilon_{T,b}}) \\ &= \frac{\sigma_{T,y}(\epsilon_{T,b}/\epsilon_{T,y})^n}{\exp[\epsilon_{T,b} + (2\nu - 1)\ \epsilon_{T,y}^{1-n}\ \epsilon_{T,b}^n]} \quad . \end{aligned} \tag{A13}$$

This is Eq. (4) in the text.